Provided for non-commercial research and education use.
Not for reproduction, distribution or commercial use.

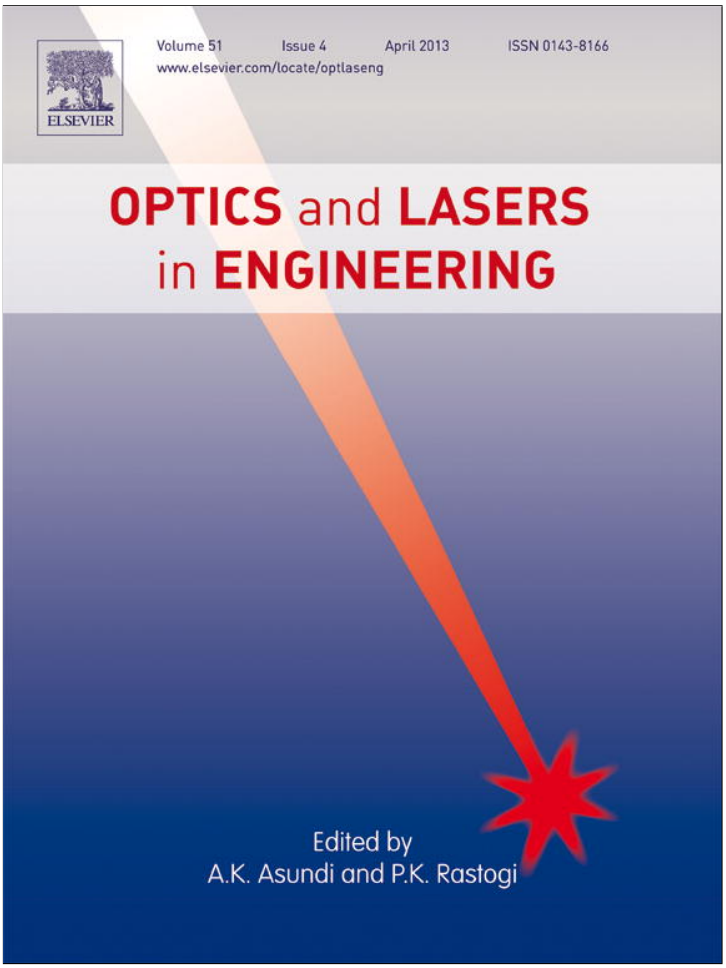

This article appeared in a journal published by Elsevier. The attached copy is furnished to the author for internal non-commercial research and education use, including for instruction at the authors institution and sharing with colleagues.

Other uses, including reproduction and distribution, or selling or licensing copies, or posting to personal, institutional or third party websites are prohibited.

In most cases authors are permitted to post their version of the article (e.g. in Word or Tex form) to their personal website or institutional repository. Authors requiring further information regarding Elsevier's archiving and manuscript policies are encouraged to visit:

http://www.elsevier.com/copyright

Author's personal copy

Optics and Lasers in Engineering 51 (2013) 342–347

Contents lists available at SciVerse ScienceDirect

Optics and Lasers in Engineering

journal homepage: www.elsevier.com/locate/optlaseng

Interferometric technique for controlling wedge angle and surface flatness of optical slabs

A.S. Andrushchak [a,b], T.I. Voronyak [b,c], O.V. Yurkevych [b], N.A. Andrushchak [b], A.V. Kityk [a,*]

[a] Department of Electrical Engineering, Institute for Computer Science, Czestochowa University of Technology, 17 Al. Armii Krajowej, Czestochowa PL-42200, Poland
[b] Lviv Polytechnic National University, 12 Bandery Street, 79013 Lviv, Ukraine
[c] Karpenko Physico-Mechanical Institute of NASU, 5 Naukova Street, 79060 Lviv, Ukraine

ARTICLE INFO

Article history:
Received 2 February 2012
Received in revised form
26 November 2012
Accepted 12 December 2012
Available online 4 January 2013

Keywords:
Interferometric technique
Optical quality control
Sample wedging measurements

ABSTRACT

We report on a laboratory setup suitable for quality control and analysis of optical slabs in the sense of perfection of their geometry and optical bulk homogeneity. Our non-contact technique based on principles of interferometry permits high-speed, precise quantitative characterization of the wedge (apex) angle and/or face flatness imperfection, as well as bulk inhomogeneity of optical slabs. The setup has been subjected to test measurements on several samples manufactured from pure and MgO-doped $LiNbO_3$ crystals for which the wedge angle and flatness deviation have been evaluated. The technique and the methodology developed by us can be offered for use in scientific research laboratories and industry.

© 2012 Elsevier Ltd. All rights reserved.

1. Introduction

Significant recent progress in many areas of optoelectronics is indebted to new advanced optical materials and relevant growth or synthesis technologies likewise material-processing methods, techniques and machineries that transform industrial materials from their raw state into finished parts or products. Optical technologies are now available to produce extremely high-quality optical elements in large quantities. Thus, any efforts aimed at increasing production and improving quality control of these elements seem to be urgent. Electro-optic and acousto-optic modulators or deflectors, nonlinear optical converters and parametric optical generators represent examples of modern optoelectronic devices. Their crucial part is an optical cell, usually a slab of a rectangular shape made of crystalline or amorphous material [1–4].

Technical characteristics of such active elements, and consequently their quality, depend much on the technology, particularly on the quality of the optical materials themselves, as well as cutting and polishing procedures used in their processing. Optical inhomogeneities of the materials caused by technological defects, strains or other structural features (e.g., domain structure, growth imperfections or inhomogeneities), and geometrical imperfections like, e.g., non-parallelism of cell faces (wedging) or deviation from their flatness (face rounding near edges) may be reflected in significant worsening of characteristics of devices. Accordingly, precise technological control of relevant parameters remains in the focus of considerable attention of many companies that deal with production of optoelectronic components and devices.

In the present work we demonstrate an interoferometric technique suitable for high-speed and precise determination of the wedge angle and the face flatness, as well as wavefront aberrations over the whole sample aperture for a light beam passing through slabs subjected to analysis. Our method complements essentially a number of other interferometric laboratory setups developed recently for precise automated determination of optical and geometrical characteristics of optical slabs made of amorphous or anisotropic materials, such as thickness and/or refractive index(ices) [5–7], piezo-optic [8–13] and electro-optic [14,15] coefficients, or acousto-optic [16,17] parameters.

2. Theoretical background

The method uses two well known principles. The first one, which is based on Snell's law, tells that a plane-parallel plate does not change the propagation direction of normally incident light which passes through it, whereas any tilt of such a plate leads only to parallel shifts of the beam. Thus, if a sample under study changes the light beam direction, this would mean that its opposite faces are not parallel and this slab can be considered as a combination of a parallel plate and a refraction prism as shown in Fig. 1(a). Actually, we deal here with a refraction prism characterized by a small apex angle ($\theta \leq 6^\circ$) usually called as an optical wedge. Although below we analyze only the simplest case

* Corresponding author. Tel.: +48 50 5895 210.
E-mail addresses: andriy.kityk@univie.ac.at, kityk@ap.univie.ac.at (A.V. Kityk).

0143-8166/$ - see front matter © 2012 Elsevier Ltd. All rights reserved.
http://dx.doi.org/10.1016/j.optlaseng.2012.12.006

Author's personal copy

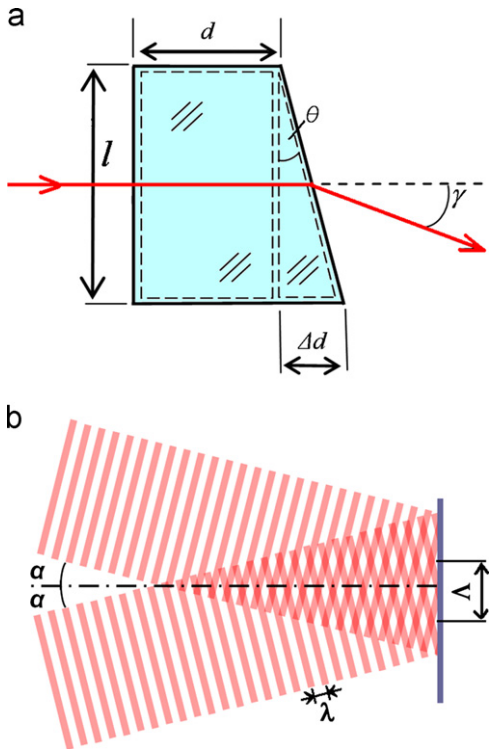

Fig. 1. Refraction of laser beam by a slab with wedge-like faces (a) and interference of two coherent laser beams projected on a screen (b).

of optically isotropic material medium, the relevant results could be trivially expanded to the case of anisotropic crystals.

Let us assume that the direction of incident light is nearly perpendicular to the sample surface. Then the deviation angle γ may be derived directly from Snell's law, resulting in the simple relation [18]

$$\gamma \approx (n-1)\theta \tag{1}$$

where n is the refractive index characterizing material of the slab. The apex angle θ and the thickness difference Δd (see Fig. 1(a)) can be determined as

$$\begin{cases} \theta = \frac{\gamma}{(n-1)}, \\ \Delta d = l\tan\theta, \end{cases} \tag{2}$$

where l is the sample aperture. To determine the deviation angle γ, the second principle should be applied. Assuming that we deal with coherent light (e.g., from laser sources), it describes the pattern caused by interference of two parallel beams. The period of this pattern, i.e. the distance between the neighbor interference fringes, Λ, is defined as [19]

$$\Lambda = \frac{\lambda}{2n_c \sin\alpha}, \tag{3}$$

where λ is the wavelength of the light, α the convergence angle (see Fig. 1(b)), and n_c the refractive index of the medium in which the coherent light beams are subjected to interference. By projecting such a pattern on the screen, one can measure its period Λ. Then the convergence angle in air ($n_{\tilde{n}} \approx 1$) can be determined as

$$\alpha = \arcsin\frac{\lambda}{2\Lambda}. \tag{4}$$

Let us consider the wedge sample shown in Fig. 1(a). The interference pattern for this particular case represents a set of equally spaced, parallel horizontal fringes. In practice the sample may be rotated about the beam by an arbitrary angle so that the interference pattern consists generally of tilted fringes. By measuring the period in the horizontal (Λ_h) and vertical (Λ_v) directions, one can determine the corresponding components of the deviation angle, γ_h and γ_v. Taking into account that $\gamma = 2\alpha$, these components are given by the relation

$$\gamma_{h,v} = 2\arcsin\frac{\lambda}{2\Lambda_{h,v}}. \tag{5}$$

As a result, the components of the wedge angle, θ_h and θ_v, and the thickness deviations Δd_h and Δd_v can be determined using the following expressions:

$$\begin{cases} \theta_{h,v} = \frac{2}{(n-1)}\arcsin\frac{\lambda}{2\Lambda_{h,v}}, \\ \Delta d_{h,v} = l_{h,v}\tan\left[\frac{2}{(n-1)}\arcsin\frac{\lambda}{2\Lambda_{h,v}}\right], \end{cases} \tag{6}$$

where l_h and l_v are the slab dimensions defining its aperture.

3. Experimental setup and method description

Our experimental setup (see Fig. 2) is based on a Mach–Zehnder interferometer (beam splitters 3 and 7, and rotating mirrors 4 and 5). It contains a single-mode He–Ne laser 1, a beam expander 2 with a spatial filter, a sample holder 6, a polarizer 11, a screen 8 on which interference pattern is projected, and a CCD camera 9 connected to a personal computer (PC) 10. The polarizer 11 is used when the geometries of each slab surface need to be analyzed separately. In this case the sample 6 is set instead of the rotating mirror 5, i.e. the slab surface itself acts as a reflecting mirror. Here the beam expander 2 forms a parallel beam with a diameter substantially exceeding the aperture of the slab. The beam splitter 3 splits the expanded beam into two beams of equal intensities, whereas the beam splitter 7 merges them again together, thereby resulting in the interference pattern projected on the screen 8. The CCD camera 9 is used to detect the interference pattern, being subjected to subsequent processing by means of the PC 10.

The analysis of the sample is held in the following order. Initially, the interferometer must be adjusted without the sample in such a manner that only one broad interference fringe (no matter which, light or dark one) is observed on the screen 8, thus leading to nearly homogeneous background illumination. In the next step the sample is placed into one of interferometer arms. A phase shift induced by the sample results in changing interference pattern, which occurs in a certain part of the expanded beam called hereafter as a sample field (see Fig. 3(a)). Evidently, this high-density fringe pattern, which originates from the light passing through the sample, is observed against a relatively

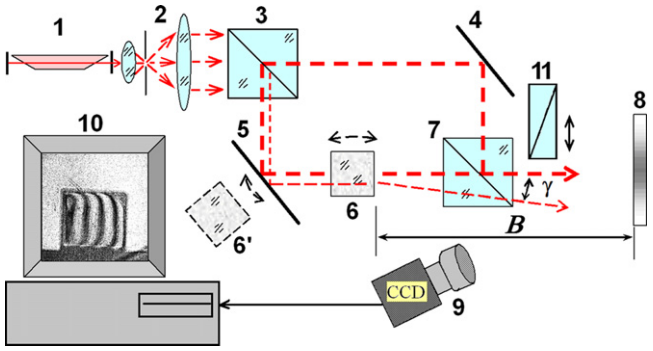

Fig. 2. Laboratory setup for controlling wedge angle and surface flatness of optical slabs: 1—laser; 2—beam expander; 3,7—beam splitters; 4,5—mirrors; 6 or 6′—sample; 8—screen; 9—CCD camera; 10—personal computer and 11—polarizer.

Author's personal copy

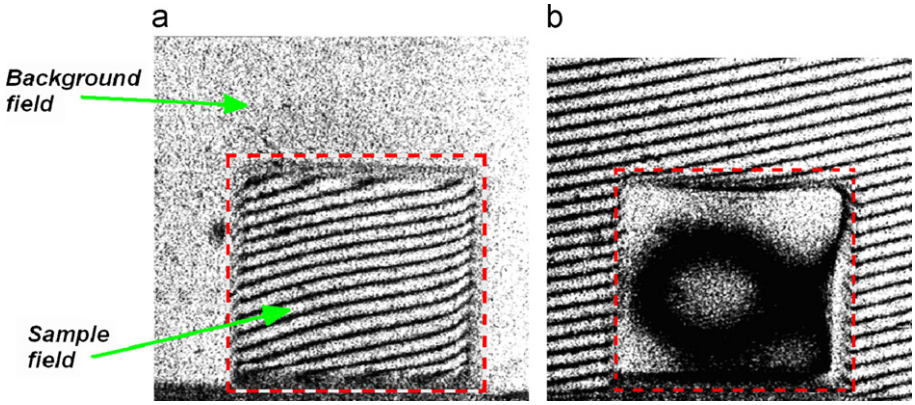

Fig. 3. Interference patterns of a sample before (a) and after (b) readjusting the interferometer.

homogeneous background illumination caused by the light propagating outside the sample (a background field). Generally speaking, the change in the interference pattern here may result from the optical bulk inhomogeneity of a material used, as well as from non-parallelism of the sample faces, i.e. sample wedging or other geometry imperfections (like, e.g., face rounding near the edges). For this reason the altered pattern is then recorded and subjected to image processing, in order to determine the spatial period components Λ_h and Λ_v. In the final step the wedge angle may be evaluated by means of Eq. (6), assuming that the refractive index n is known.

To assess the other sample imperfections (e.g., the face flatness imperfection or inhomogeneity of optical properties across the aperture of the crystal sample), it is necessary to readjust the interferometer. By rotating the mirror 5, the beam passing through the sample has to be redirected parallel to the reference beam. This increases the spatial period (or decreases the number of fringes) for the interference pattern observed in the sample field. On the other hand, it will simultaneously increase the density of fringes observed within the background field. Therefore the pattern becomes in the end very similar to that observed in the sample field before readjustment of the interferometer (compare Fig. 3(a) and (b)). If the fringes disappear completely within the sample field, i.e. the pattern finally looks there as a homogeneously illuminated field, then one deals with an optically homogeneous sample having perfectly flat opposite faces which, at the same time, are not necessarily parallel to each other.

Thus by measuring the spatial period of the interference pattern within the background field (see Fig. 3(b)) one may determine again the sample wedging. Analyzing the sample field in Fig. 3(b), one may conclude that either one surface or both slab surfaces are not perfectly flat or the sample is spatially inhomogeneous, which may be caused by a number of reasons (e.g., low optical quality of the raw material or mechanical strains that occur during processing of this material). To distinguish between different reasons, the surface flatness should be analyzed separately for each face in the reflected light, i.e. by replacing the mirror 5 with the sample (see Fig. 2). Then only the geometry imperfections of the surface would be explored. Performing comparative analysis of different interference patterns, one may conclude on whether the remaining interference fringes within the sample field (see Fig. 3(b)) are geometrical or/and bulk imperfections.

Special attention has to be given to the case where the sample wedging is very large so that the resulting high-density interference pattern cannot be resolved by the CCD camera (see Fig. 4). In such situation one should measure components of the beam shift in the horizontal and vertical directions, A_h and A_v, as well as the distance between the sample and the screen, B (see Fig. 2).

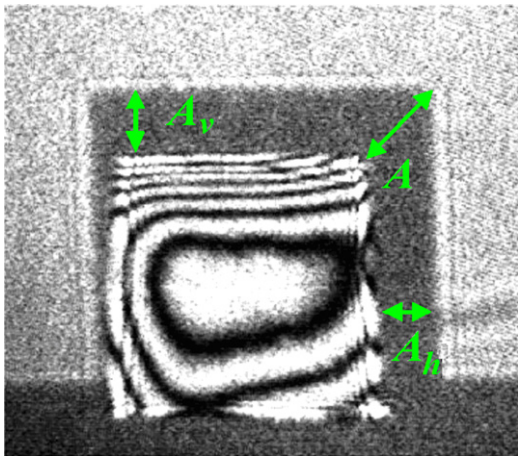

Fig. 4. Interference pattern of a sample characterized by a large wedge angle between the opposite faces.

The components of the deviation angle are then determined as

$$\gamma_{h,v} = \arctan\frac{A_{h,v}}{B}. \tag{7}$$

Thus one must use a couple of fairly similar equations

$$\begin{cases} \theta_{h,v} = \frac{1}{(n-1)}\arctan\frac{A_{h,v}}{B}, \\ \Delta d_{h,v} = l_{h,v}\tan\left[\frac{1}{(n-1)}\arctan\frac{A_{h,v}}{B}\right], \end{cases} \tag{8}$$

instead of Eq. (6). In particular, Fig. 4 shows the interference pattern for the case of very large wedge angle. Components of the beam shift in the horizontal and vertical directions, A_h and A_v, are labeled here.

4. Experimental results

In this section we present test measurements on several samples, using the laboratory setup and the methodology described above. For this aim, boules (Ø=50 mm) of the pure $LiNbO_3$ and MgO-doped $LiNbO_3$ single crystals have been subjected to processing (including crystallographic orientation by means of the X-ray technique and consequent cutting and polishing procedures), in order to prepare slabs with the dimensions of approximately $10\times10\times12$ mm^3. Two samples of different crystallographic orientations, which represent a direct crystal cut (the faces are perpendicular to the principal X, Y or Z axes) and a 45°/X cut, have been chosen for further interferometric analyses. The quality of material processing procedures has been

Author's personal copy

intentionally chosen to be different for different faces. Thereby the interferometric analysis has had as its purpose characterizing the geometry imperfections quantitatively. Figs. 5 and 6 present the interference patterns for the direct and the 45°/*X* cuts, respectively. They have been captured when the monochromatic laser light ($\lambda=633$ nm) passes through the samples along the three different crystallographic directions associated with the actual orientation directions of the slab faces (see the labels). Here the left and right panels correspond to the two different settings in the interferometer setup used during the analysis as described in the previous section (see Figs. 2 and 3, as well as the relevant explanation). Already a first glance at these patterns gives an idea about the features and the scale of the geometrical imperfections for each of those particular cases. The larger the fringe density, the larger the wedge angle between the opposite faces, and vice versa. The distortion of the interference pattern, which is observed near the edges, suggests that, in addition to the face wedging, we deal also with imperfectly flat faces, i.e. their geometry is characterized by roundings near the edges. Subsequent image processing allows describing such a kind of sample imperfections quantitatively. In our evaluations we rely on the refractive indices for the $LiNbO_3$ (or $LiNbO_3 \cdot MgO$) crystals, $n_o=2.2865$ (or 2.2841) and $n_e=2.2034$ (or 1.2994) as measured with the interferometric method [20] for the direct crystal cut. The effective refractive index calculated for the 45°/*X* cut sample is $n_4 = n_{\bar{4}} = \sqrt{2}/\sqrt{n_o^{-2}+n_e^{-2}}=2.2438$ for $LiNbO_3$ and 2.2406 for $LiNbO_3 \cdot MgO$. The total apex angle θ characterizing the face wedging may be evaluated as $\theta=(\theta_h^2+\theta_v^2)^{1/2}$, where θ_h and θ_v are the wedge angle components calculated using Eq. (6) and the interference pattern periods measured along the horizontal and vertical directions, respectively. The angle θ determined this way, as well as its components, θ_h and θ_v, is labeled in Figs. 5 and 6 for each of the presented particular cases. One can see that the angle θ depends notably on the quality of mechanical processing. It ranges from 37.5″ for the 45°/*X* cut (the light wave vector $q||4$, where 4 implies the diagonal *Y*–*Z* direction, see Fig. 6(b)) down to 3′16.4″ for the direct cut ($q||Z$,see Fig. 5(c)). The distortion of the interference fringes near the sample edges is relevant to their shift from about one half to a whole inter-fringe spacing. In the assumption that both faces are rounded nearly equally, this roughly corresponds to the deviation from perfect flatness at the edges, $\Delta d_{edg}=(0.5\div 1)\lambda/(2(n-1))$, i.e. in the range from 0.12 to 0.25 μm for each face in average. For a more explicit characterization, the surface flatness should be explored separately for each face, while replacing the mirror 5 with the sample (see Fig. 2). Patterns recorded in such a way may be also used

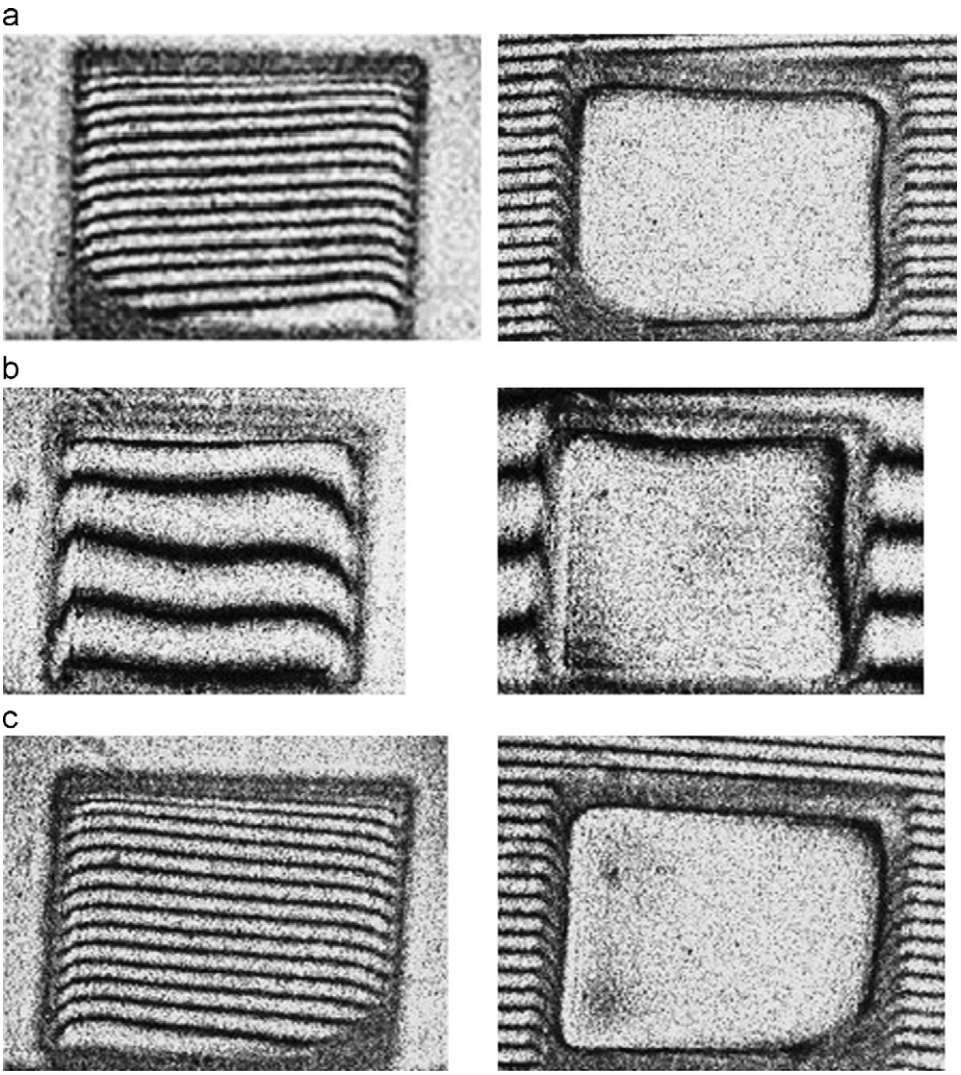

Fig. 5. Interference patterns for rectangular crystal sample of pure $LiNbO_3$ (direct cut) obtained along the principal crystallographic directions (see labels) by means of interferometric setup of Fig. 2. Left and right panels correspond to different adjustments of laser beam direction *q* (see explanations in text): (a) $q||X$; $\theta=2'43.2''$ ($\theta_h=7''$; $\theta_v=2'43''$, $h||Y$, $v||Z$); (b) $q||Y$; $\theta=45.2''$ ($\theta_h=4''$; $\theta_v=45''$, $h||Z$, $v||X$) and (c) $q||Z$; $\theta=3'16.4''$ ($\theta_h=12''$; $\theta_v=3'16''$, $h||Y$, $v||X$).

Author's personal copy

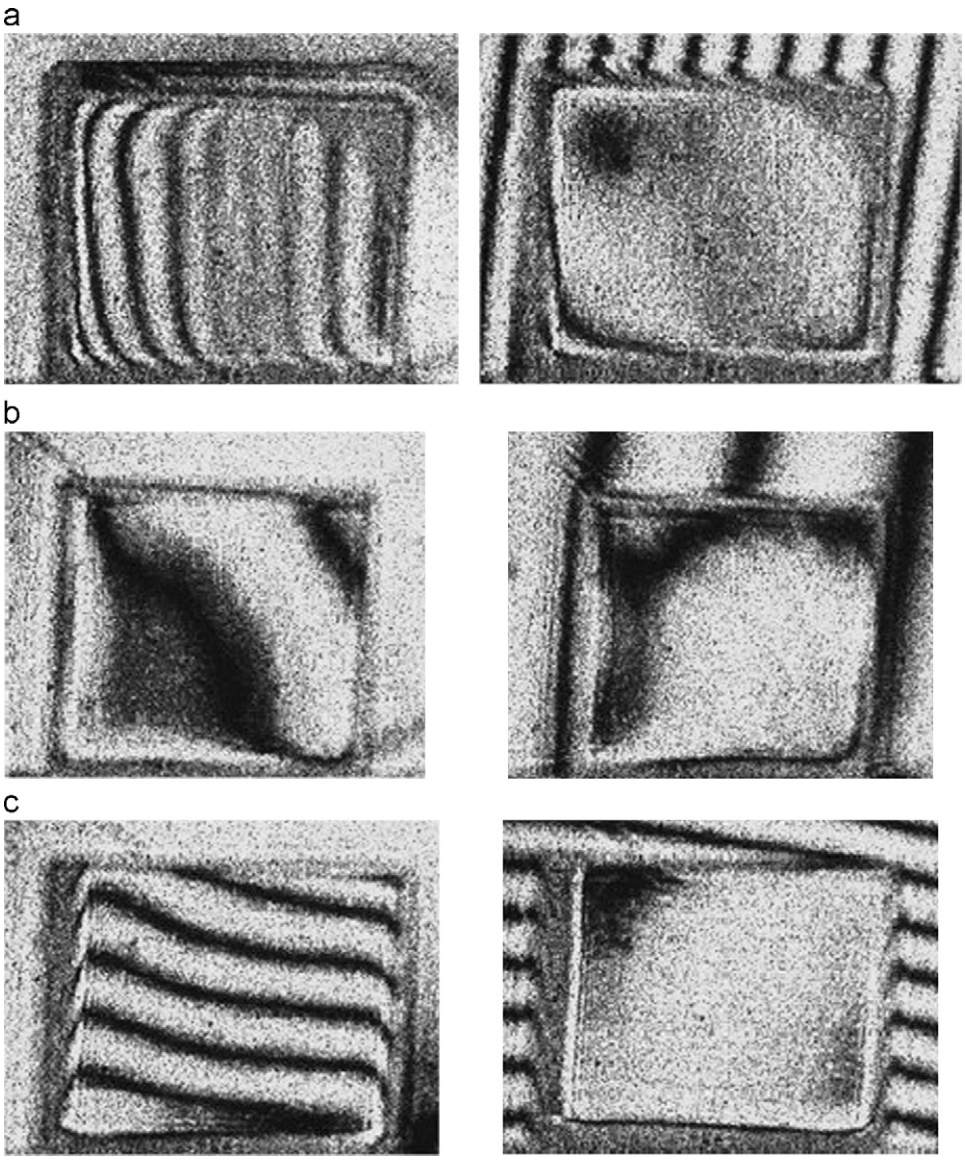

Fig. 6. Interference patterns of rectangular crystal sample of MgO-doped $LiNbO_3$ (45°/*X* cut) obtained along the principal crystallographic directions (see labels) by means of interferometric setup of Fig. 2. Left and right panels correspond to different adjustments of laser beam direction q (see explanations in text): (a) $q||X$; $\theta=1'12''$ ($\theta_h=1'11''$; $\theta_v=11''$, $h||4$, $v||\overline{4}$); (b) $q||4$; $\theta=37.5''$ ($\theta_h=37''$; $\theta_v=6''$, $h||X$, $v||\overline{4}$) and (c) $q||\overline{4}$; $\theta=1'7''$ ($\theta_h=12''$; $\theta_v=1'6''$, $h||4$, $v||X$).

for subsequent image processing aimed at getting a 3D profile of the surface.

5. Conclusions

Taking together, we have presented here a laboratory setup suitable for the quality control and quantitative analysis of optical slabs in the sense of their geometry perfection and optical bulk homogeneity. Being based on the Mach–Zehnder interferometer, such a non-contact technique is able to give both fast and precise quantitative characterization of the face wedging and/or flatness imperfection, together with the wavefront aberrations of optical slabs. By applying different settings in the interferometer setup, which include interferometric analyses in the transmitted and reflected light, one can separate well the geometrical imperfections relevant with the faces wedging and the deviations from flatness. Our setup has been subjected to the test measurements performed on several samples manufactured from both pure $LiNbO_3$ and the same crystals doped with MgO, for which the wedging angles and the deviations from flatness have been evaluated. The technique and the methodology developed here can be suitable for scientific research laboratories and industry.

Acknowledgment

This work was supported by the Marie Curie International Incoming Fellowship within the 7th European Community Framework Program (Project no. 272715).

References

[1] Shackelford JF. Introduction to materials science for engineers, 6th Ed. New Jersey: Pearson Prentice Hall; 2005, 878 p.
[2] Günter P, Huignard JP. Photorefractive materials and their applications. Berlin: Springer; 2007, 640 p.
[3] Narasimhamurty TS. Photoelastic and electro-optic properties of crystals. New York: Plenum; 1981, 514 p.
[4] Korpel A. Acousto optics, 2nd Ed. New York: Marcel Dekker; 1996, 240 p.

Author's personal copy

[5] Andrushchak AS, Tybinka BV, Ostrovskij IP, Schranz W, Kityk AV. Automated interferometric technique for express analysis of the refractive indices in isotropic and anisotropic optical materials. Opt Laser Eng 2008;46:162–7.
[6] Wang J, Strausser S. Single-photon determination of transmission, index of refraction and material thickness. J Mod Opt 2012;59:381–6.
[7] Zhang J, Xu JQ, Gao CY, Si SC. Modified Michelson interferometer for probing refractive index of birefringent crystal CSBN50. Opt Laser Eng 2009;47: 1212–5.
[8] Mytsyk BG, Andrushchak AS. Ambiguity of principal coordinate system choice in studies of the piezo-optical effect in $LiNbO_3$ crystals. Kristallografiya 1990;35:1574–5.
[9] Andrushchak AS, Mytsyk BG, Lyubych OV. Piezo-optical indicative surfaces in lithium niobate crystals. Ukr Fiz Zh 1992;37:1217–24.
[10] Krupych O, Savaryn V, Skab I, Vlokh R. Interferometric measurements of piezo-optic coefficients by means of four-point bending method. Ukr J Phys Opt 2011;12:150–9.
[11] Vasylkiv Yu, Savaryn V, Smaga I, Skab I, Vokh R. Determination of piezo-optic coefficient π_{14} of $LiNbO_3$ crystals under torsion loading. Ukr J Phys Opt 2010;11:156–64.
[12] Andrushchak AS, Mytsyk BG, Laba HP, Yurkevych OV, Solskii IM, Kityk AV, et al. Complete sets of elastic and photoelastic constants of pure and MgO doped lithium niobate crystals at room temperature. J Appl Phys 2009;106: 073510.
[13] Mytsyk BG, Andrushchak AS, Demyanyshyn NM, Kost' YP, Kityk AV, Mandracci P, et al. Piezo-optic coefficients of MgO doped $LiNbO_3$ crystals. Appl Opt 2009;48:1904–11.
[14] Andrushchak AS, Mytsyk BG, Demyanyshyn NM, Kaidan MV, Yurkevych OV, Solskii IM, et al. Spatial anisotropy of linear electro-optic effect for crystal materials: I. Experimental determination of electro-optic tensor by means of interferometric technique. Opt Laser Eng 2009;47:31–8.
[15] Nava G, Minzioni P, Yan W, Parravicini J, Grando D, Musso E, et al. Electro-optical coefficients and refractive indices of Zr-doped $LiNbO_3$ crystals. Opt Mater Express 2011;1:270–7.
[16] Kotov VM, Shkerdin GN, Shkerdin DG, Kotov EV. Contouring of images by means of the bragg acousto-optical diffraction into two orders. J Commun Technol Electron 2011;56:52–5.
[17] Andrushchak AS, Chernyhivsky EM, Gotra Yu Z, Kaidan MV, Kityk AV, Andrushchak NA, et al. Spatial anisotropy of the acoustooptical efficiency in lithium niobate crystals. J Appl Phys 2010;108:103118.
[18] Gvozdeva NP, Korkina KI. The theory of optical systems and optical measurements. Moscow: Mashinostroenie; 1981 (in Russian).
[19] Zakaznova NP, editor. Applied optics. Moscow: Mashinostroenie; 1988 (in Russian).
[20] Andrushchak AS, Mytsyk BG, Demyanyshyn NM, Kaidan MV, Yurkevych OV, Dumych SS, et al. Spatial anisotropy of linear electro-optic effect for crystal materials: II. Indicative surfaces as efficient tool for electro-optic coupling optimization. Opt Laser Eng 2009;47:24–30.